THE GEOLOGICAL SOCIETY OF AMERICA®

Effects of Igneous Intrusions on Coal Pore Structure, Methane Desorption and Diffusion within Coal, and Gas Occurrence

MING-YI CHEN
YUAN-PING CHENG[1]
HONG-XING ZHOU
LIANG WANG
FU-CHAO TIAN
KAN JIN

National Engineering Research Center for Coal & Gas Control, China University of Mining & Technology, Xuzhou 221116, China, and Key Laboratory of Gas and Fire Control for Coal Mines, China University of Mining & Technology, Xuzhou 221116, China; mingyichen@cumt.edu.cn

Key Terms: ***Mining Geology, Igneous Rock, Coal and Gas Outburst, Coal Seam Gas Occurrence***

ABSTRACT

Igneous intrusions are distributed extensively in the Huaibei coalfield, China. In the Haizi coal mine, coal and gas outbursts have occurred 11 times under an extremely thick sill (average thickness 120 m). This paper presents the results of a study on the influences of the igneous rock on coal pore structure, methane desorption and diffusion properties, and coal seam gas occurrence. The results show that the thermal evolution effect of the igneous sill prominently increases the specific surface area and pore volume of the affected coal. Samples HZ1 and HZ2 (No. 7 and No. 9 seams, respectively) closer to the sill possess improved pore connectivity, while samples HZ3 and HZ4 (away from the sill) and sample HZ5 (without sill covering) of the No. 10 coal seam have poor pore connectivity. Moreover, the effective diffusivity and desorption indexes of the coal increase progressively closer to the sill. The thermal effect of the igneous sill promotes the development of coal pores, thus leading to better pore connectivity, more desorbed gas, and much higher gas desorption and diffusion rates. Consequently, the thermal evolution effect of the igneous sill can change the occurrence and characteristics of the entrapment effect in the underlying coal seams, thus resulting in a high probability of gas hazards or even coal and gas outbursts in the coal seam close to the igneous sill. Engineering practices show that the affected coal seams have high gas content, gas pressure, and gas emission amounts as well as a high propensity for coal and gas outburst.

[1]Corresponding author email: ypcheng@cumt.edu.cn.

INTRODUCTION

Coal measure strata intruded by igneous rock can be found in many coalfields worldwide. Igneous intrusion activity changes the properties of the coal, such as their petrographic, maceral, and geochemical properties, resulting from the thermal effects associated with the intrusions (Finkelman et al., 1998; Golab and Carr, 2004; Stewart et al., 2005; Dai and Ren, 2007; Rimmer et al., 2009; Yang et al., 2012; Chen et al., 2014; and Rahman and Rimmer, 2014). The changes in the physicochemical properties of coal depend on the distance between the coal and the igneous intrusions, the duration of magmatic-derived heat, and the temperature of the intrusions, among other factors (Cooper et al., 2007; Wu et al., 2014). In general, with an increase in the metamorphic grade of coal affected by intruding magma, the porosity and adsorption capacity of the coal are enhanced, thus increasing its gas storage capacity (Saghafi et al., 2008). Meanwhile, a significant quantity of gas may be trapped in the coal seams by the magmatic rock, which can cause potential problems regarding mining safety when working with the affected coal seams. Many studies have suggested that such gas hazards are closely related to igneous intrusions (Jiang et al., 2011; Sachsenhofer et al., 2012; Wang et al., 2014b, 2014d; and Xu et al., 2014).

The thermal effect of the intrusions has a significant impact on the pore structure of the coal (Mastalerz et al., 2009; Yao and Liu, 2012; and Wu et al., 2014), and it also influences the gas adsorption property and gas flow characteristics of the coal (Saghafi et al., 2008; Yao et al., 2011). Igneous intrusions have been identified as an important factor in abnormally high gas emissions (Shepherd et al., 1981; Xu et al., 2014). Previous research focused more on the changes in the pore parameters, such as pore volume and porosity, as well as in the gas adsorption capacity of the coal in the

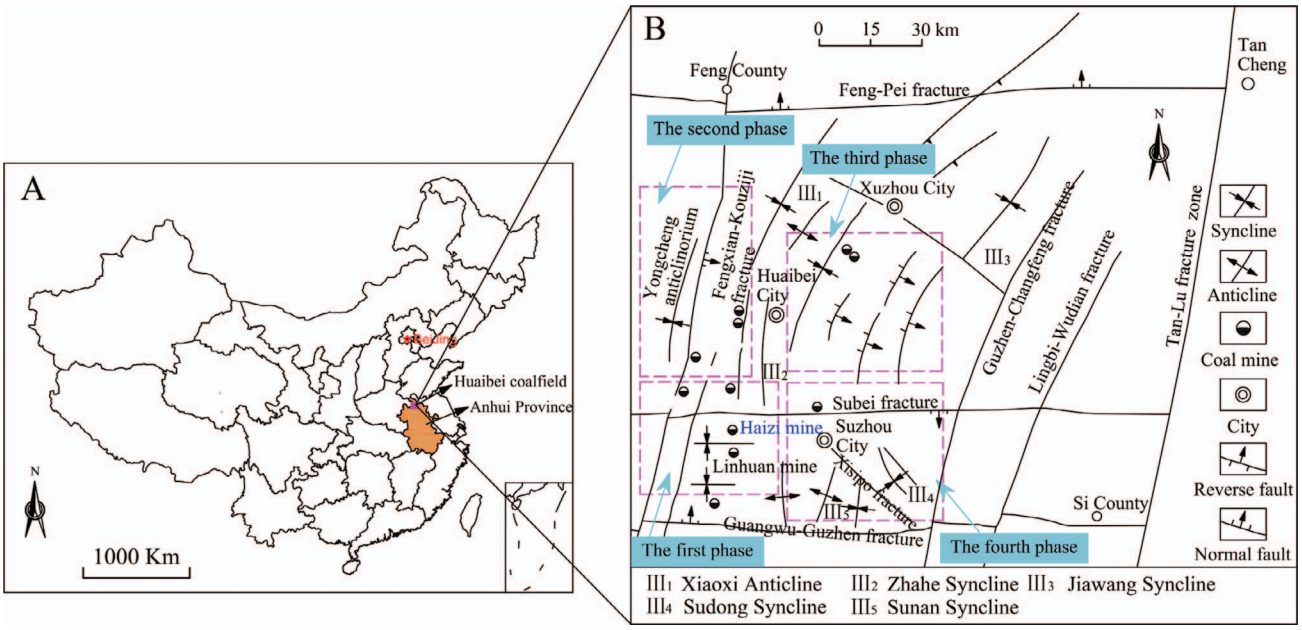

Figure 1. The location of the Huaibei coalfield (A) and structural outline map (B).

affected area. Correspondingly, there has been a lack of investigation regarding the pore structure and its influences on the gas desorption and diffusion properties of coal under the thermal effect from the igneous intrusions. The pore structure of coal changes the gas adsorption and flow capacities of coal (An et al., 2013; Cai et al., 2013), both of which also have a significant impact on coal and gas outbursts (Skoczylas et al., 2014; Jian et al., 2015). In China, several prediction indexes associated with gas desorption and diffusion properties within coal are generally used for the prevention and control of outburst hazards in coal mines (Cheng et al., 2010; Cheng et al., 2016). Therefore, it is reasonable to perform a study to understand the change in pore structure and its impact on gas desorption and diffusion properties of coal under the influence of intrusive thermal effects.

Magmatic activity is frequent and widespread within the Huaibei coal field, China. The Haizi coal mine lies in the middle of the Huaibei coalfield in Anhui Province, where igneous intrusions are extensively distributed and have caused 11 coal and gas outbursts, all of which occurred under an extremely thick sill. Many studies have since been conducted on the coal seam gas occurrence, the disaster-causing mechanisms of the intrusions, and the prevention and control of coal and gas outbursts in the Haizi mine (Wang et al., 2013; Chen et al., 2014; Wang et al., 2014a, 2014b, 2014c, 2014d; and Zhang et al., 2015). Based on these studies, this paper is focused on determining the influence of the thermal effect of an igneous sill on pore structure, including pore size distribution and pore shape, methane desorption and diffusion properties, and the impact of pore structure on these properties in an underlying coal seam. It is important to understand the influence of the igneous sill on coal seam gas occurrence and gas hazards in the Haizi mine. Moreover, these results can provide theoretical guidance for coal mines with similar geological conditions to prevent and control gas hazards.

MAGMATIC INTRUSIONS IN THE HAIZI MINE

As shown in Figure 1A, the Huaibei coalfield is located in northern Anhui Province with an area of approximately 13,000 km^2. Through multi-stage tectonic movement, it has formed complex fold and fault systems (Qu et al., 2008). It has also experienced many periods of magmatic activity. Magmatic activity was the most active during the Mesozoic Yanshan epoch and caused the greatest damage synchronous with coal metamorphism in the coalfield (Han, 1990; Yang et al., 1996). As shown in Figure 1B, Han (1990) divided Yanshanian magmatic intrusions into four phases. The first phase was composed of neutral magmatic rock, the magmatism of the second phase was intermediately acidic, the third phase contained acidic magmatic rock, and the fourth phase was composed of basic and ultrabasic magmatic rock.

As shown in Figure 2A, the Haizi coal mine is bordered by the Damajia Fault and the Linhuan mine to the southeast, and the Daliujia Fault to the west in the Huaibei coalfield of Anhui Province, China.

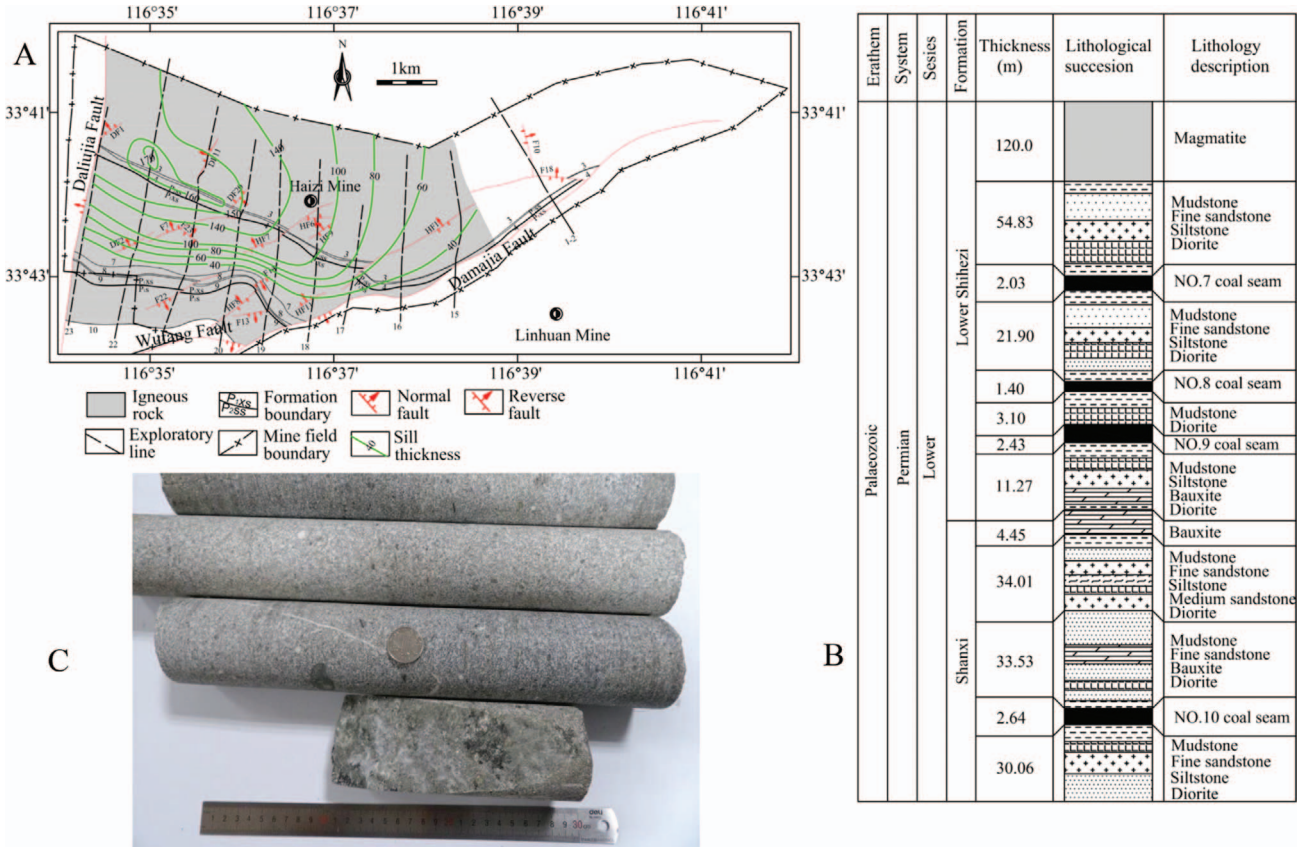

Figure 2. (A) Map of igneous intrusion distribution in the Haizi coal mine. (B) Histogram of coal-bearing strata of the II102 mining area in the Haizi coal mine. (C) Photos of igneous rock.

Its regional geological structure is closely related to the Subei Fault. The magmatic evolution in the Haizi mine can be summarized as follows. During the Yanshan epoch, deep crustal magma upwelled along the Subei Fault zones and subsequently flowed into the Daliujia Fault through the hanging wall of the Subei Fault and then invaded the Haizi coal mine from north to south. The intrusive magma continued to invade fault fracture zones connected with the Daliujia Fault. Finally, the magma invaded the coal-bearing strata along the coal seam roof and floor and even engulfed coal units such as the No. 5 coal seam. The igneous intrusions in the Haizi mine primarily include dikes and sills; igneous intrusions in sills are the most common.

The maximum thickness of the igneous sill is approximately 170 m, the sill length along its strike is 6.5 km, and the average thickness of the sill is 120 m. This sill is the most stable in the II102 mining area. A histogram of coal-bearing strata in the II102 mining area of the Haizi mine is shown in Figure 2B, wherein the Nos. 7, 8, 9, and 10 seams are the primary mineable coal beds in the Permian strata. The igneous intrusions are distributed as a sill over the coal seams. This super-thick igneous sill occurs above and nearly parallel to the minable coal seams. It maintains great influence on the metamorphism and gas occurrence of the underlying coal seams.

The igneous rock samples are shown in Figure 2C. They are characterized by a hard and complete structure with a porphyritic texture and light gray to grayish-green appearance. The igneous rocks of the Haizi mine are neutral, being chiefly composed of diorite and diorite porphyrite (Wang et al., 2014b). The magmatic activity in the Haizi mine area is interpreted to be related to the first phase of Yanshan magmatic activity.

EXPERIMENTAL WORK

Sampling and Basic Physical Parameters of Samples

Beneath the sill, the underlying coal seams are characterized by high gas pressure and gas content, which pose an outburst hazard. In addition, compared with the gas content of the No. 10 seam, the Nos. 7, 8, and 9

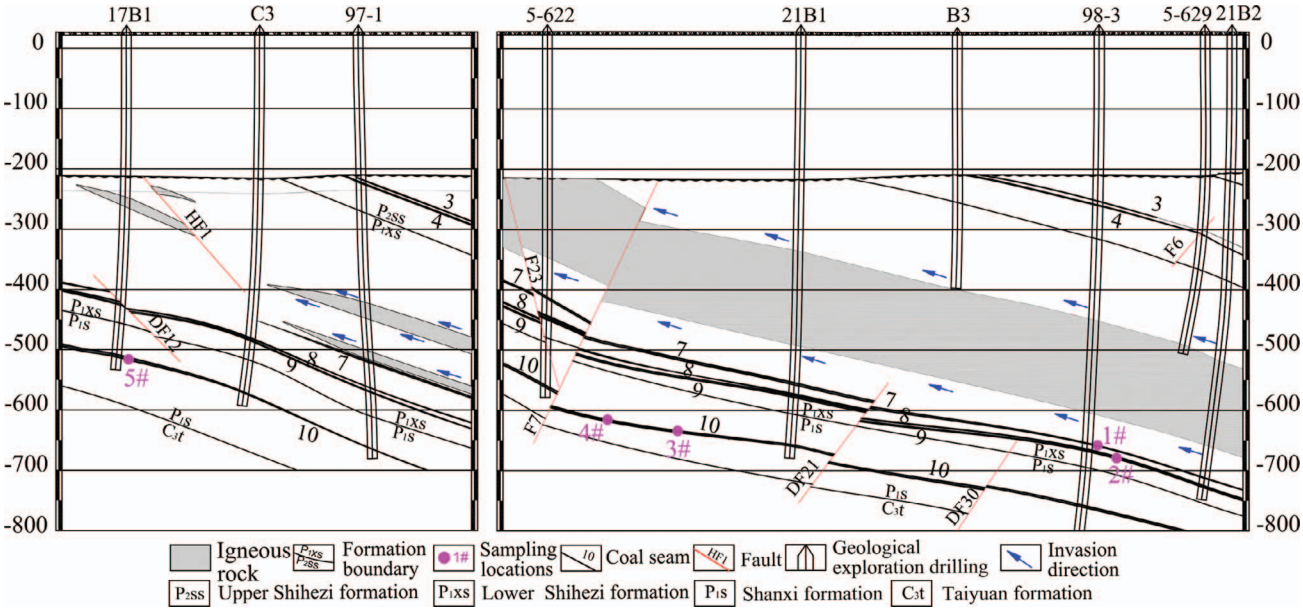

Figure 3. Cross sections showing the sampling locations.

seams have greater value and also exceed the outburst prediction critical value of 8 m^3/t (Cheng et al., 2010). As shown in Figure 3, four samples were taken from the Nos. 7, 9, and 10 seams in the mining area with the sill covering (where the sill thickness is approximately 140 m), which are located in the outburst risk region. A sample was collected from a non-outburst risk region of the No. 10 seam in the mining area without the sill covering for comparison.

There are significant differences in the basic physical properties among the five samples. The physical parameters of the samples from the corresponding coal seams are listed in Table 1. The proximate analysis roughly reflects the quantities of inorganic and organic matter in the samples, which was performed by using an automatic proximate analyzer following the ISO 17246:2010 standard. The vitrinite reflectance mainly reflects the degree of coal metamorphism, which was determined by following the ISO 7404-5:2009 standard. The Langmuir constant V_L reflects the adsorption capacity of coal for gas, which was determined by following the GB/T 19560-2008 standard. The initial velocity of methane diffusion (Δp) was determined by following the AQ1080-2009 standard.

As shown in Table 1, the maximum vitrinite reflectance ($R_{o,\,max}$) beneath the igneous sill varies from 1.25 percent (HZ4) to 2.74 percent (HZ1), and the ash content (A_{ad}) ranges from 8.17 percent to 26.46 percent, with the higher values being closer to the igneous sill. The volatile matter (V_{daf}) ranges from 8.92 percent (HZ1) to 13.5 percent (HZ4), with the higher values being farther away from the sill. Sample HZ1, which is closest to the sill, has an abnormally high moisture value (M_{ad}, 2.02 percent). This high value is likely caused by the igneous sill creating a sealing effect that traps the moisture from the thermal metamorphism of coal.

Figure 4 illustrates the trends in both the maximum vitrinite reflectance ($R_{o,\,max}$) and the Langmuir constant V_L of coal, which tend to increase closer to the sill. The sample closest to the sill, HZ1, has the largest metamorphic grade ($R_{o,\,max}$ = 2.74 percent) and methane adsorption capacity (V_L = 45.12 cm^3/g), whereas sample HZ5, located in an area without sill covering, has the lowest values ($R_{o,\,max}$ = 0.66 percent and V_L = 17.80 cm^3/g).

Therefore, the thermal evolution effect of the igneous sill significantly increases the metamorphic grade of coal close to the igneous intrusions. The methane adsorption capacities are also considerably enhanced, which are related to the influence of the thermal evolution effect on the development of coal porosity.

Experimental Methods

The physical gas adsorption method (using N_2 as the probe molecule) is used extensively for analyzing pore characteristics of porous substances (Nie et al., 2015; Okolo et al., 2015). N_2 adsorption/desorption isotherms at 77 K were obtained using a Quantachrome Autosorb-iQ2 for particle sizes in the range of 0.2–0.25 mm. The relative pressure (P/P_0) was

Table 1. *Summary of physical parameters of analyzed samples.*

Sample	Coal Seam	Distance from Sill (m)	Elevation (m)	$R_{o,max}$ (%)	Proximate Analyses (%)			Langmuir Constant		Δp (mm Hg)
					M_{ad}	A_{ad}	V_{daf}	V_L (cm^3/g)	P_L (MPa)	
HZ1	7	55	−660	2.74	2.02	26.46	8.92	45.12	1.09	45.0
HZ2	9	70	−680	2.20	0.54	19.18	12.56	37.09	1.12	31.8
HZ3	10	152	−635	1.72	1.29	11.29	13.13	34.97	0.86	17.2
HZ4	10	156	−618	1.25	1.28	8.17	13.5	28.34	1.04	12.6
HZ5	10	Without sill covering	−515	0.66	0.68	11.9	21.63	17.80	1.19	5.8

observed over the range from 0.001 to 0.995. Pore parameters were automatically calculated via computer software named ASIQwin™. The Brunauer-Emmett-Teller (BET), Barrett-Joyner-Halenda (BJH), and quenched solid state density functional theory (QS-DFT) methods were used for determining the pore volume, specific surface area (SSA), and pore size distribution (PSD). A detailed discussion of these methods can be obtained from the publication of Lowell et al. (2012). Prior to the experiments, the coal samples were placed in a vacuum drying oven and then dried at 60°C for at least 24 hours.

The bulk desorption method (Zhang, 2008) was used to obtain the methane desorption data (methane desorbed volume versus time) of coal with particle sizes of 0.5–1 mm and 1–3 mm. Each sample was weighed at 50 g and then placed in a coal sample jar. The gas tightness of all coal sample jars was verified. Next, the jars were placed in a thermostatic water bath at 333 K and then evacuated using a vacuum pump for 24 hours. Subsequently, the jars were filled with pure methane and then placed in a thermostatic water bath at 303 K for at least 48 hours. To obtain the required gas pressures of 2 MPa, excessive free gas was released during the methane adsorption equilibrium process. Once the gauge pressure of the coal sample jars remained constant, the methane desorption tests were started. A stopwatch was used to record the time to methane desorption, which occurred when the gas within each of the jars was simultaneously and instantaneously relieved. Methane desorption data were recorded for a period of 2 hours. A detailed description of the methane desorption tests also can be found in the publication of Liu et al. (2015).

Desorption Equation

Many gas desorption models and equations have been proposed and employed to calculate coal seam methane contents. The equation $Q_t = K_1\sqrt{t}$, which

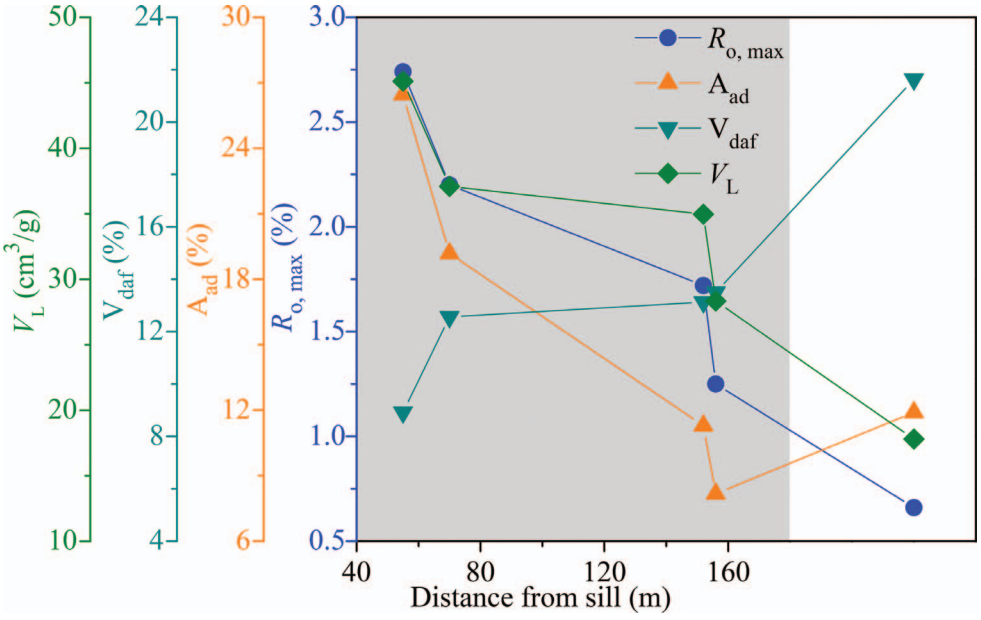

Figure 4. Variations in multiple physical parameters of the coal samples with distance from the igneous sill.

is also called the Barrer-type equation, is the most common equation used to estimate the initial lost-gas volume (Diamond and Schatzel, 1998). However, the equation is not well suited for data in long gas desorption tests. The Airey-type and Winter-type equations are commonly used to study the gas desorption law of pulverized coal. By assuming gas desorption from a solid exhibiting a cracked structure, the gas desorbed volume discharged at time t can be found by Eq. 1 (Airey, 1968):

$$Q_t = A\left[1 - \exp\left\{-\left(\frac{t}{t_0}\right)^n\right\}\right], \quad (1)$$

where Q_t is the gas desorption volume at time t, mL/g; A is the ultimate desorption volume, mL/g; t_0 is the desorption time constant; and n is a coefficient.

In Winter's theory, the desorption rate of methane from coal grains versus time can be described and fitted by Eq. 2 (Winter and Janas, 1975):

$$V_t = V_a\left(\frac{t}{t_a}\right)^{-k_t}. \quad (2)$$

After mathematical integration, the following equation of gas desorption volume and time is obtained:

$$Q_t = \frac{V_1}{1 - k_t} t^{1-k_t}, \quad (3)$$

where Q_t is the gas desorption volume at time t, mL/g; V_1 and V_a are the rates of gas desorption at times t_1 and t_a, respectively, mL/(g·min); and k_t is a constant that reflects the degree of attenuation of the desorption rate and characterizes the gas desorption law (Banerjee, 1988).

Diffusion Equation

According to Fick's law and by assuming a spherical and homogeneous solid with a constant radius and smooth surface, the unipore model is derived as the following equation (Crank, 1979):

$$\frac{M_t}{M_\infty} = 1 - \frac{6}{\pi^2}\sum_{n=1}^{\infty}\frac{1}{n^2}\exp\left(-\frac{D}{r^2}n^2\pi^2 t\right), \quad (4)$$

where M_t is the total amount of diffusion media through the sphere within time t; M_∞ is the total desorbed quantity; D is the diffusion coefficient; and r is the mean radius of the sphere particles. D_e can be obtained using the equation $D_e = D/r^2$ (Marecka and Mianowski, 1998), where D_e is the effective diffusivity.

Equation 4 can be rewritten as the following equation:

$$\frac{Q_t}{Q_\infty} = 1 - \frac{6}{\pi^2}\sum_{n=1}^{\infty}\frac{1}{n^2}\exp(-D_e n^2\pi^2 t), \quad (5)$$

where Q_t is the total volume of desorbed gas diffusing through the coal particles within time t, mL/g; and Q_∞ is the total volume of gas desorbed, mL/g. Q_∞ can be determined from experimental methods (Chen and Cheng, 2015; Lu et al., 2015) and can also be determined by Eq. 1, being equal to the ultimate desorption volume A in Eq. 1.

RESULTS

Pore Analysis by the N_2 Adsorption Method

N_2 Adsorption and Desorption Isotherms and Pore Shapes

N_2 adsorption and desorption isotherms for the five coal samples are illustrated in Figure 5. All of the adsorption isotherms are type II, exhibiting multi-layer adsorption. Sample HZ1, closest to the igneous sill, adsorbed the most N_2, while sample HZ5, without the sill covering, adsorbed the least N_2 at the highest relative pressure, suggesting that sample HZ1 has a larger micro-porosity and adsorption capacity.

Six characteristic types of hysteresis loops are provided by the International Union of Pure and Applied Chemistry (IUPAC) (Thommes et al., 2015), which are based on the original IUPAC classification of 1985. As shown in Figure 5, except for sample HZ1, the plots demonstrating the change in volume with respect to the P/P_0 ratio for adsorption and desorption are essentially coincident for all the samples when the relative pressure (P/P_0) is less than 0.45, suggesting that the smaller pores are mainly in the shapes of pores accessible via a single pore throat (Zhang et al., 2013). When the P/P_0 exceeds 0.5, a distinct hysteresis loop can be observed in the isotherms of samples HZ1 and HZ2, indicating the presence of a large number of open pores and corresponding to better pore connectivity in the two samples. This conspicuous hysteresis is ascribed to the difference between condensation and evaporation processes in the coal pores (Mastalerz et al., 2012; Yang et al., 2014). According to the classification of IUPAC, the hysteresis loops of samples HZ1 and HZ2 belong to type H3 and may indicate the presence of numerous slit-shaped pores, the existence of which is thought to be a significant internal factor for causing coal and gas outburst hazards (Jiang et al., 2011). The desorption branch of sample HZ2 shows a sudden drop in the volume with a forced closure of the hysteresis loop at a relative pressure of approximately 0.45

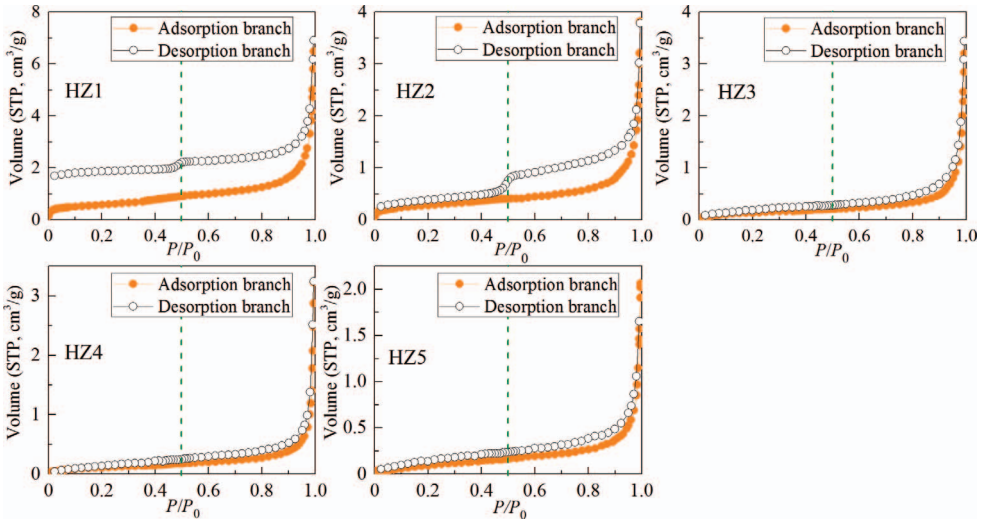

Figure 5. N_2 adsorption/desorption isotherms of coal samples at 77 K.

because of the so-called tensile strength effect (TSE) (Groen et al., 2003; Lowell et al., 2012). An abrupt change in volume also exists in the desorption branch of sample HZ1. However, the hysteresis loop is still observed at a relative pressure of less than 0.45 for sample HZ1, which is more likely to be the result of adsorption swelling of the coal (Kondo et al., 2005; Cai et al., 2013). The adsorption and desorption branches are essentially coincident for samples HZ3, HZ4, and HZ5, suggesting the existence of many semi-closed pores that may, for instance, include cylindrical and slit-shaped pores with one closed side in the coals, indicating poor pore connectivity. This phenomenon is in accordance with the research results in the publication of Nie et al. (2015).

Pore Volume and Specific Surface Area

The pore volume and SSA of the coal samples from the nitrogen adsorption tests at 77 K were calculated using the BET, BJH, and QSDFT methods, as shown in Table 2. The pore volume and SSA of sample HZ1 closest to the sill are the largest, whereas those of the unaffected coal sample HZ5 are the smallest. On the basis of the IUPAC classification (Thommes et al., 2015), pores are divided into the following three categories: macro-pores (≥50 nm), meso-pores (2–50 nm) and micro-pores (≤2 nm). A micro-pore analysis using the CO_2 adsorption method for the No. 9 and No. 10 coal seams obtained from sample locations similar to ours can be obtained from the publication of Wang et al. (2014a). Figure 6 illustrates a dramatic decrease in both the pore volume and SSA of micro-pores, meso-pores, and macro-pores for the samples closer to the sill. Sample HZ5 has the lowest values of SSA and pore volume. In the study of Wang et al. (2014a), numerous thermally metamorphic pores in the coal samples closer to the extremely thick sill were depicted using a scanning electron photomicrograph; in contrast, only a few such pores were found in the samples away from the sill, and no pores were found in the samples of the unaffected coals. Research shows that thermally metamorphic pores are formed during the devolatilization of liptinite and vitrinite (Sarana and Kar, 2011). Therefore, under the thermal effect of the intrusions, both

Table 2. *Pore volume and specific surface area of coal samples from nitrogen adsorption at 77 K.*

Sample No.	BET SSA (m^2/g)	BJH SSA (m^2/g)	BJH Pore Volume[a] ($\times 10^{-3}$ cm^3/g)	QSDFT Volume[b] SSA[b] (m^2/g)	QSDFT Pore ($\times 10^{-3}$ cm^3/g)	QSDFT Pore Diameter[b] (nm)
HZ1	2.054	1.440	10.200	1.764	3.894	1.193
HZ2	1.015	0.595	5.609	0.798	2.000	1.144
HZ3	0.522	0.412	5.227	0.401	1.523	1.682
HZ4	0.423	0.303	4.830	0.308	1.042	1.756
HZ5	0.405	0.295	3.048	0.279	0.896	4.077

[a]Pore diameter ranges from 3 to 300 nm.
[b]Pore diameter ranges from 0.9 to 35 nm.

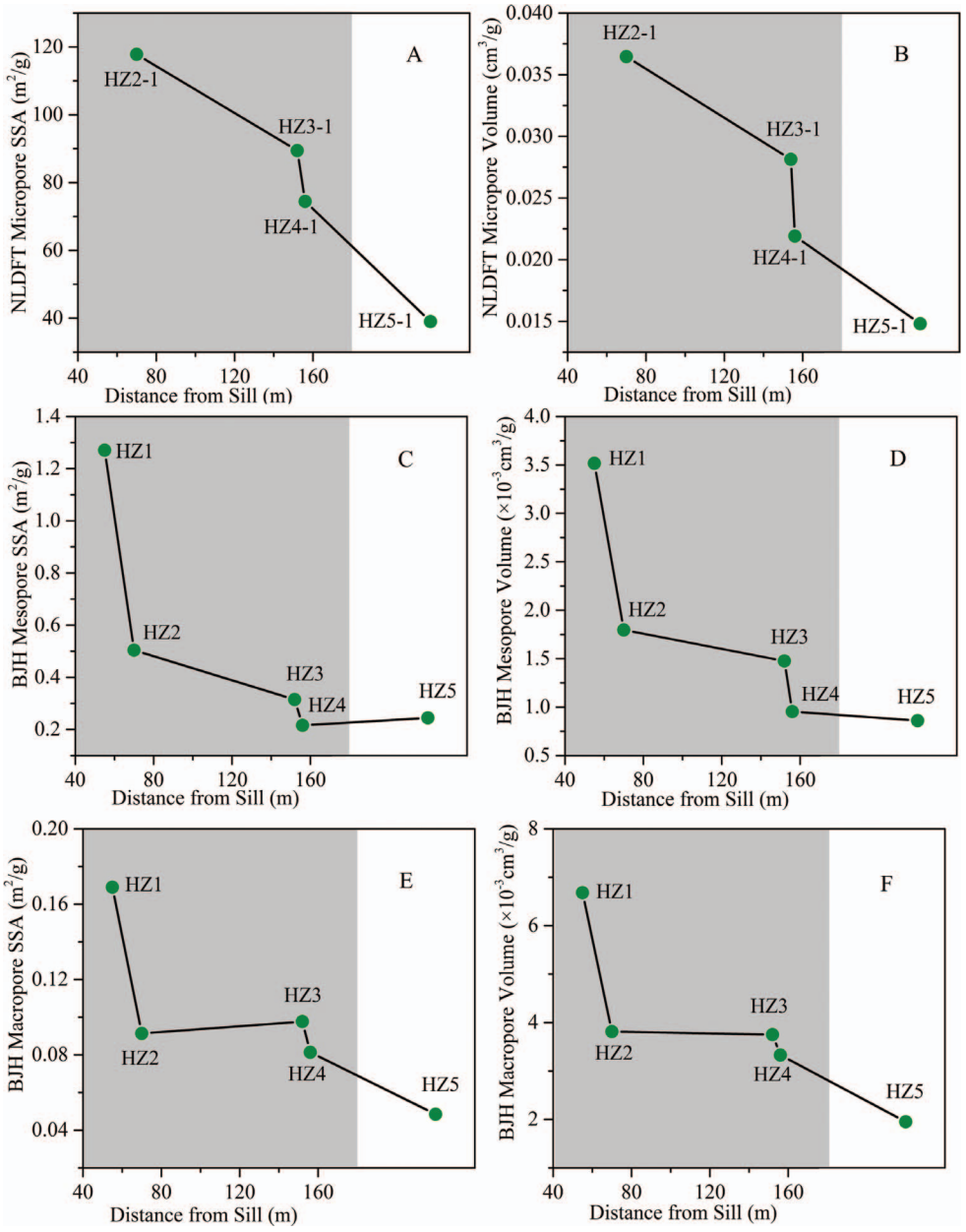

Figure 6. Changes in specific surface area (SSA), and pore volume of coal samples with the distance from the sill. Micro-pore SSA and volume (A and B) were calculated using the Non-Local Density Functional Theory (NLDFT) model, where the pore diameter ranged from 0.35 to 1.50 nm (Wang et al., 2014a). Sample HZ2-1 is from the No. 9 coal seam, samples HZ3-1, HZ4-1, an HZ5-1 are from the No. 10 coal seam, and sample HZ5-1 is from the unaffected area. The meso-pore SSA and volume were calculated using the BJH model (C and D). The macro-pore (50–300 nm) SSA and volume were calculated using the BJH model (E and F). The gray zone represents the area with sill coverage.

the pore volume and SSA increase dramatically in the coal samples approaching the sill. The prominent enhancement of micro-pore volume and SSA leads to an increase in the gas adsorption and storage capacities, which can increase the risk of coal and gas outbursts during mining activity in the coal seams closer to the sill.

Pore Size Distributions

Plots of the PSDs (Figure 7) show that uni-modal or multi-modal PSDs exist in the range of 1–100 nm for all coal samples. The QSDFT $dV(d)$ plots (Figure 7A) suggest a bi-modality for sample HZ1 (peaks at ~1 nm and ~4 nm), whereas the BJH $dV(d)$ plots (Figure 7B)

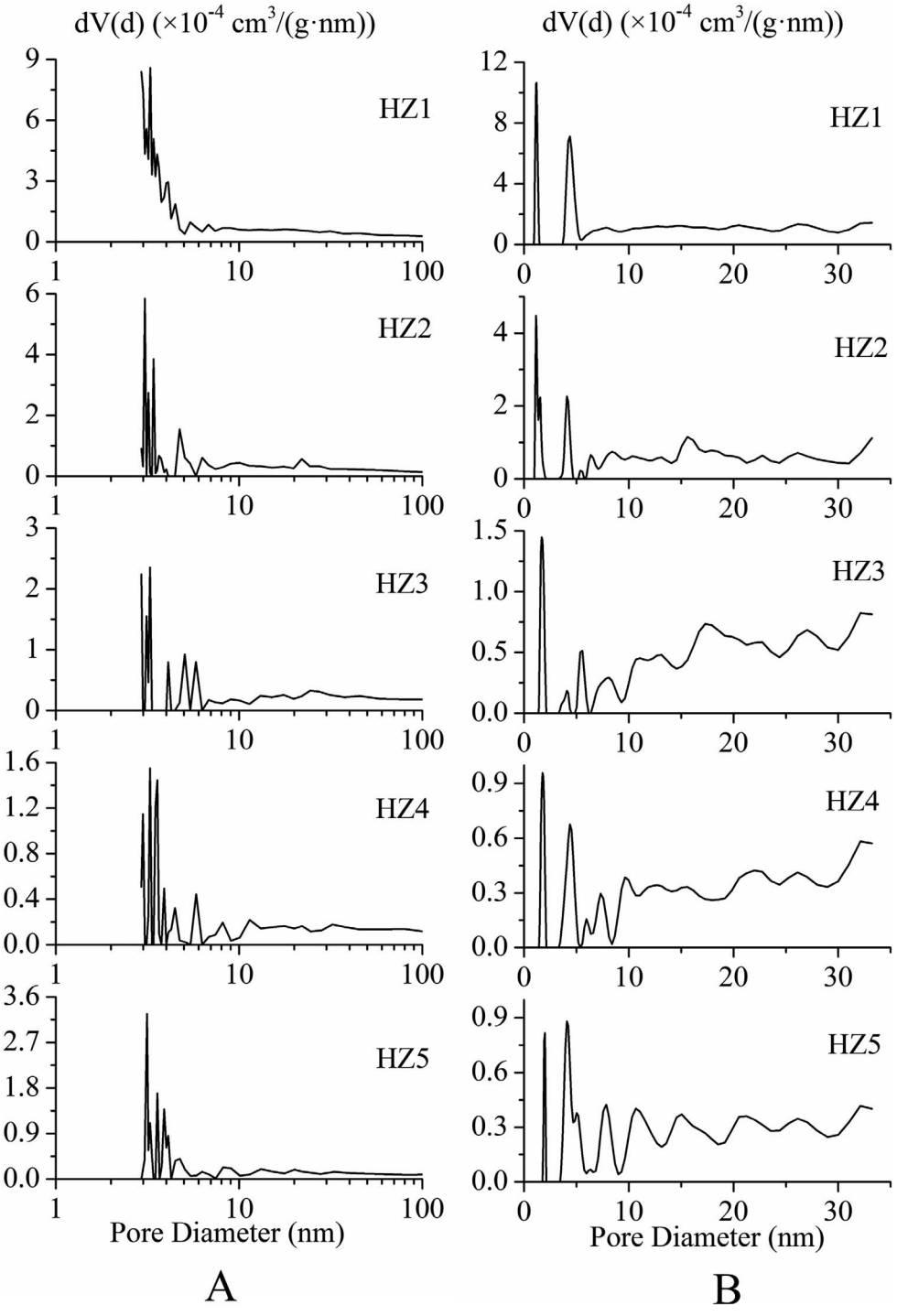

Figure 7. Pore size distributions (PSDs) using QSDFT (A) and BJH (B).

suggest uni-modality with a peak at <4 nm. Sample HZ2 appears to exhibit bi-modality, with peaks at ~1 nm and ~4 nm (Figure 7A) and peaks at ~3 nm and ~5 nm (Figure 7B). Both the QSDFT $dV(d)$ and the BJH $dV(d)$ plots reveal multi-modality for samples HZ3, HZ4, and HZ5. The major peaks exist in pores <5 nm for samples HZ1 and HZ2, suggesting the enhancement of the SSA and volume of micro-pores and some meso-pores. This result indicates a prominent increase in the gas adsorption and storage capacities of coals closer to the igneous sill. The pore volumes of samples HZ3 and HZ4 both exhibit relatively small increases in the

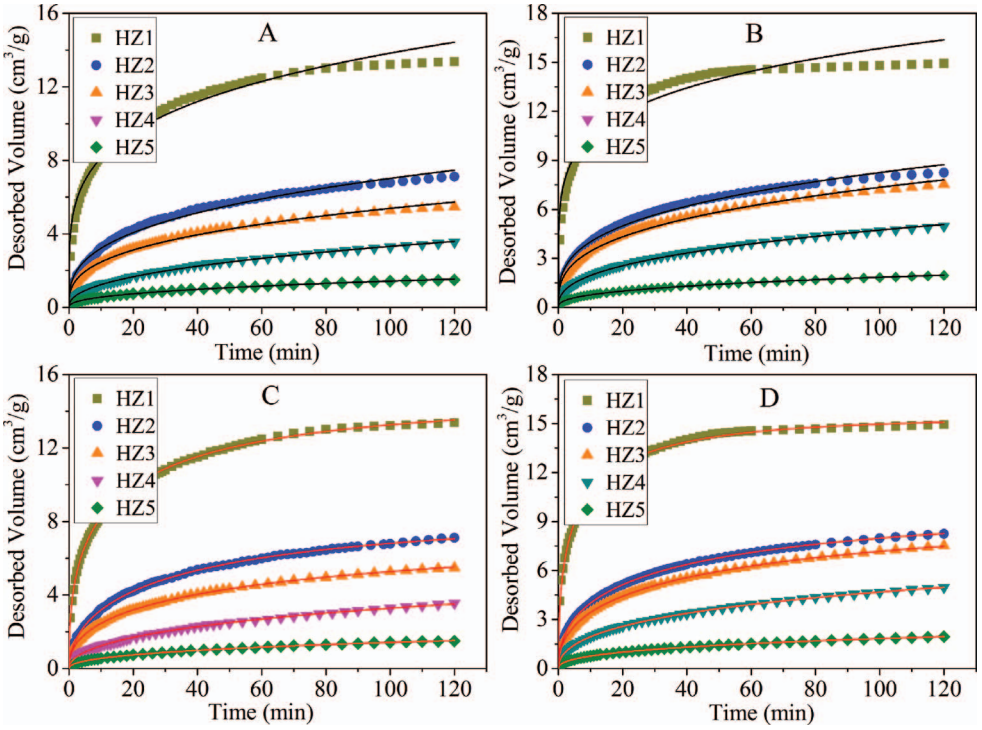

Figure 8. Winter-type equation fitting curves of methane desorption data for the coal particles in the ranges of 1–3 mm (A) and 0.5–1 mm (B), and Airey-type equation fitting curves of methane desorption data for the coal particles in the ranges of 1–3 mm (C) and 0.5–1 mm (D).

range of 1–30 nm, indicating that the thermal effect has a weaker effect on pore development of coal farther away from the sill. Samples HZ5, HZ3, and HZ4 show similar PSD behaviors.

Methane Desorption Index and Effective Diffusivity

Fitted curves of methane desorption data for the coal particles (1–3 mm and 0.5–1 mm) using Eq. 1 and Eq. 3 are shown in Figure 8. The results are summarized in Table 3. Both the Airey-type and the Winter-type equations have high values of the correlation coefficient R^2, suggesting a high-fitting precision. For the samples with particle sizes in the range of 1–3 mm, the ultimate desorption volume A varies from 4.50 to 15.30 cm^3/g, the initial desorption rate V_1 ranges from 0.088 to 1.103 $cm^3/(min{\cdot}g)$, and the initial desorption volume K_1 varies from 0.194 to 3.679 cm^3/g. Sample HZ1 closest to the sill shows the largest initial desorption volume and rate (19.0 times and 12.5 times, respectively, greater than that of sample HZ5). In addition, the smaller-sized samples have larger initial values for the volume and rate of desorption, likely because of the heterogeneity of coal.

The results of the effective diffusivity of the coal samples calculated using Eq. 5 are listed in Table 4. For the coal samples with particle sizes in the range of 1–3 mm, the effective diffusivity D_e varies from 1.980×10^{-6} to $4.626 \times 10^{-5}\ s^{-1}$, and the effective diffusivity of sample HZ1 is 12.53 times greater than that of sample HZ5. Therefore, both the methane desorption amounts and effective diffusivity of the samples increase significantly closer to the sill. The enhancements in the gas desorption and diffusion properties of the coals are likely due to the significant influence of the thermal effect of the sill on the pore structure of the coal.

DISCUSSION

Change in Methane Effective Diffusivity

On the basis of the Knudsen number, the gas diffusion within a coal pore system is primarily divided into Fick diffusion, Knudsen diffusion, and transitional diffusion (Li et al., 2012). Note that two other diffusion types, surface diffusion and crystal diffusion, are not often considered in coalbed methane studies (Nie et al., 2000). The Knudsen number (K_n) is expressed as the ratio of the pore diameter (d) of the coal matrix to the mean molecule free path (λ). The mean molecule free path is represented by the following equation:

$$\lambda = \frac{KT}{\sqrt{2}\pi d_0^2 p}, \tag{6}$$

Table 3. *Fitting results for the methane desorption indexes.*

Sample	Particle Size	Airey-Type Equation				Winter-Type Equation			
		A (cm^3/g)	t_0 (min)	n	R^2	V_1 [$cm^3/(min{\cdot}g)$]	k_t	R^2	K_1[a] (cm^3/g)
HZ1	1–3 mm	15.30	18.37	0.420	0.9991	1.103	0.769	0.9774	3.679
	0.5–1 mm	16.16	8.50	0.427	0.9960	1.245	0.820	0.9472	5.414
HZ2	1–3 mm	8.39	39.05	0.543	0.9996	0.499	0.666	0.9885	1.115
	0.5–1 mm	10.07	40	0.491	1	0.611	0.687	0.9883	1.443
HZ3	1–3 mm	7.94	83	0.469	0.9980	0.383	0.660	0.9938	0.902
	0.5–1 mm	10.12	64.41	0.475	1	0.530	0.670	0.9938	1.276
HZ4	1–3 mm	7.89	350	0.498	0.9993	0.201	0.585	0.9982	0.387
	0.5–1 mm	9.89	260.1	0.467	1	0.309	0.615	0.9985	0.705
HZ5	1–3 mm	4.50	834	0.460	0.9996	0.088	0.591	0.9992	0.194
	0.5–1 mm	5.08	640.9	0.438	0.9998	0.121	0.618	0.9992	0.296

[a] K_1 represents the gas desorption volume in the first minute, and the K_1 value is the measured result rather than a fitted value.

where K is the Boltzmann constant, 1.38×10^{-23} J/K; T is the absolute temperature, K; d_0 is the effective diameter of gas molecules, nm; and p is the gas absolute pressure, MPa.

When K_n is larger than 10, collisions are predominantly inter-molecular collisions between gas molecules due to the pore diameter being far greater than the mean molecule free path. In this case, Fick diffusion is the dominant diffusion mechanism. When K_n is larger than 0.1, collisions are primarily between gas molecules and coal pore walls because the pore diameter is much less than the mean molecule free path. Thus, Knudsen diffusion is the main gas diffusion mechanism. When K_n is between 0.1 and 10, collisions between gas molecules and collisions between gas molecules and pore walls are of equal importance. As such, transitional diffusion is the dominant diffusion mechanism.

Considering Eq. 6, when the experiment temperature is 30°C (303.15 K), the mean molecule free path for methane is 86.5 nm in the case when the pressure of the coal sample jar is instantaneously relieved ($p = 0.1$ MPa). Based upon previous studies, it is known that the effective distance of a coal surface interacting with a methane molecule is approximately 0.55 nm, corresponding to a pore diameter of approximately 1.10 nm and a distance of the adsorption potential well of approximately 0.36 nm (Jiang et al., 2006). Additionally, the effective diameter of the methane molecule is approximately 0.33 nm. Hence, owing to the influence of the coal surface, surface diffusion occurs in the coal pores when the diameter ranges from 0.33 to 1.1 nm (Xu et al., 2015).

Table 4. *Results of effective diffusivity using the unipore model.*

Sample	Particle Size (mm)	D_e (s^{-1})	R^2
HZ1	1–3	4.626×10^{-5}	0.8911
	0.5–1	9.205×10^{-5}	0.8901
HZ2	1–3	2.268×10^{-5}	0.9896
	0.5–1	2.344×10^{-5}	0.9699
HZ3	1–3	1.313×10^{-5}	0.9677
	0.5–1	1.591×10^{-5}	0.9689
HZ4	1–3	3.482×10^{-6}	0.9956
	0.5–1	4.976×10^{-6}	0.9836
HZ5	1–3	1.980×10^{-6}	0.9700
	0.5–1	2.623×10^{-6}	0.9753

As illustrated in Figure 9, Knudsen diffusion is the chief diffusion type in pores with a size range of 1.1–8.65 nm, whereas transitional diffusion occurs in pores with a size range of 8.65–865 nm, and Fick diffusion occurs in pores when the pore diameter exceeds 865 nm. A pore diameter of 100 nm is generally considered to be a cutoff point for gas diffusion and seepage in coal by many scholars (Hodot, 1966). Given this cutoff point and regardless of surface diffusion, pores with a size range of 1.1–100 nm may represent the primary spaces for methane diffusion. Hence, under the experimental conditions (i.e., pressure is completely relieved, p is 0.1 MPa, and T is 303.15 K), the main diffusion modes are Knudsen diffusion and transitional diffusion.

The relationship between the effective diffusivity (D_e) and a volume of pores with a size range of 1.1–100 nm is shown in Figure 10. As illustrated in Figure 10A, a pore volume with a size range from 1.1 to 100 nm can be calculated by the sum of the volume of pores in the size range of 1.1–8.65 nm (QSDFT) and 8.65–100 nm (BJH). Sample HZ1, having a size range of 1.1–100 nm, has the largest pore volume and effective diffusivity (5.442×10^{-3} cm^3/g and 46.26×10^{-6} s^{-1}, respectively), while sample HZ5 has the smallest (1.317×10^{-3} cm^3/g and 1.98×10^{-6} s^{-1}). The effective diffusivity and pore volume within the size range of 1.1–100 nm increase progressively closer to the sill. Figure 10B exhibits a positive correlation between the pore volume with a size range of 1.1–100 nm and methane effective diffusivity.

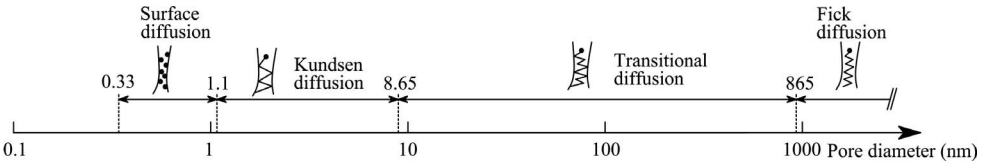

Figure 9. The diffusion modes in the corresponding pore diameter range under the experimental conditions ($p = 0.1$ MPa and $T = 303.15$ K).

Relationships between Methane Desorption Index and Pore Characteristics

The igneous sill provides a high-temperature environment that promotes the thermo-metamorphism of coal and the formation of coal-bed gas (Wang et al., 2014c). Coupled with the entrapment effect of the extremely thick sill, the amount of gas released is reduced while large amounts of gas are stored in the affected coal seams. The presence of a larger number of micro-pores in coal can significantly increase the gas adsorption capacity of coal. Thus, more gas can be released at the moment of pressure relief under the same circumstances. More importantly, well-developed meso-pores and macro-pores can provide broad pore channels for gas diffusion and seepage; on the other hand, better pore connectivity favors gas migration from the coal matrix to fractures. Hence, the impact of the thermal effect of the sill on the pore structure of coal increases the risk of outburst accidents during mining of the coal seam. During the history of the Haizi mine, coal and gas outbursts have occurred five times in the No. 7 seam, once within the No. 9 seam, and once within the No. 10 seam under the extremely thick sill. Experience demonstrates that the No. 7 seam closest to the igneous sill has a greater risk of coal and gas outburst.

The indexes K_1, Δp, and k_t are effective parameters with which to predict the risk of coal and gas outbursts (Du, 1985; Cheng et al., 2010). Figure 11A shows the variations in the desorption indexes K_1, Δp, and k_t of the samples (1–3 mm) relative to distance from the igneous sill. The K_1 index varies from 0.194 to 3.679 cm^3/g, the Δp index ranges from 5.8 to 45.0 mm Hg, and the k_t index ranges from 0.585 to 0.769, with the higher values observed closer to the igneous sill. There is an increasing trend in the values of the K_1 and Δp indexes as the distance to the sill decreases. Hence, due to the thermal evolution effect of the sill, larger SSA and pore volumes as well as better pore connectivity are found in coals closer to the sill, which leads to a greater initial gas desorption volume and rate (K_1 and Δp) than in coals situated farther away from the sill or in unaffected coals. Figure 11B indicates that the k_t index is positively related with macro-pore volume because k_t is considered to be the desorption rate attenuation index characterizing the ratio between the gas desorption volume in the macro-pores and the micro-fractures in the first minute after the gas pressure is relieved (Guo et al., 2014). Note that sample HZ5 (No. 10 seam) from the non-outburst risk region and sample HZ4 from the outburst risk region (No. 10 seam) have similar values of k_t, likely because the k_t index is independent of the gas pressure in the coal seam (Du, 1985).

Effects of the Igneous Sill on Coal Seam Gas Occurrence in the Haizi Mine

Figure 12A shows the distribution of igneous sills in the II101 and II102 mining areas. The thermal

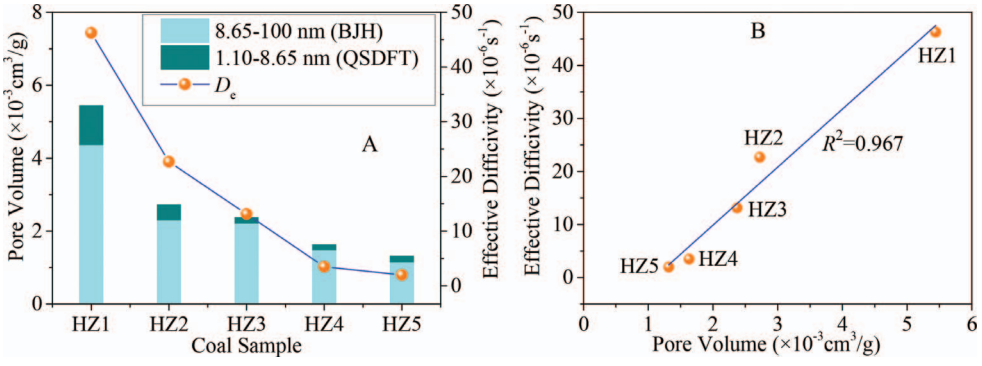

Figure 10. Variations of the effective diffusivity and the total volume of the pores in the ranges of 1.1–8.65 nm (QSDFT) and 8.65–100 nm (BJH) for the coal samples (A), and the relationship between the pore volume in size range of 1.1–100 nm and the methane effective diffusivity (B).

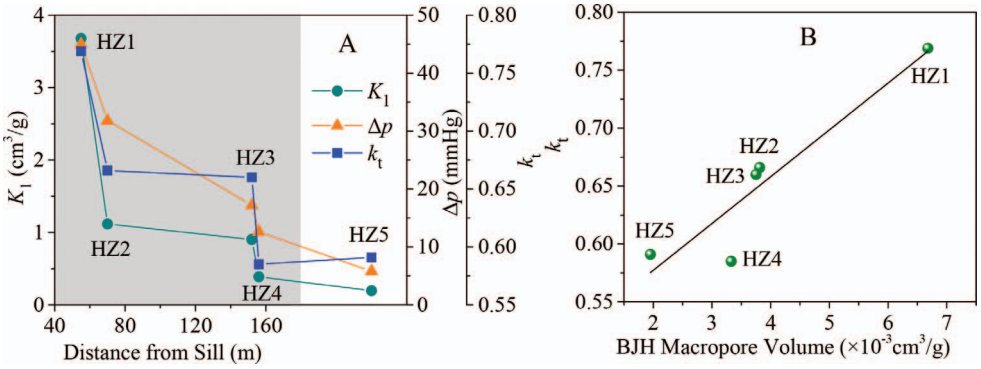

Figure 11. Variation in the methane desorption indexes of the samples (1–3 mm) with distance from the sill (A) and the relationship between the K_t index and the BJH macro-pore volume (B).

impact from igneous intrusions is greater for the II102 mining area, which possesses a substantially thicker sill, compared to the II101 mining area, which has few sill coverings. The measured results of gas content and gas pressure of the No. 10 coal seam in the two mining areas are shown in Figure 12B and Figure 12C, respectively. The results show that the No. 10 coal seam in the II102 mining area has a relatively higher coal seam gas content and greater gas pressure gradient (0.0374 MPa/m). Figure 12D indicates that more gas is

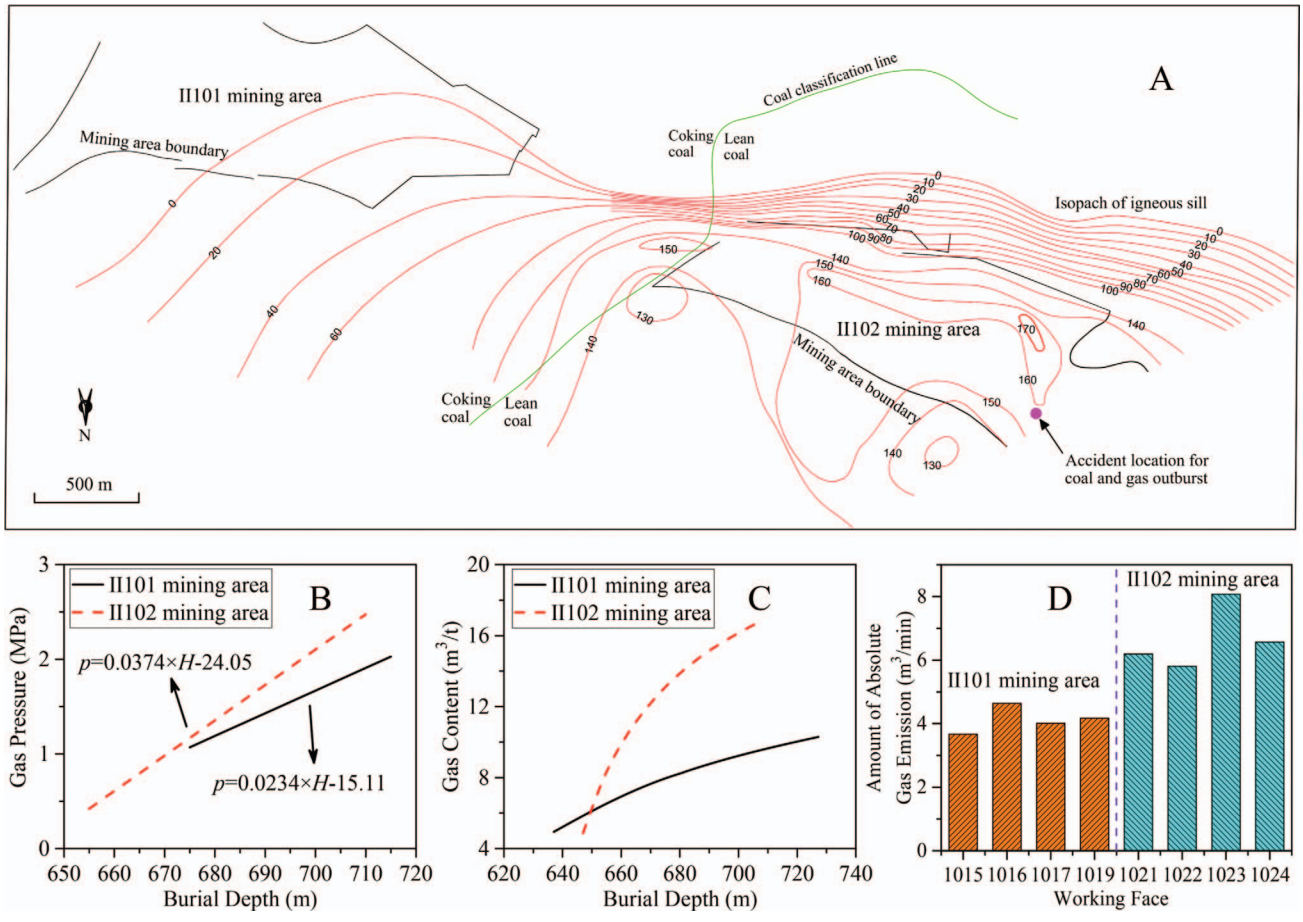

Figure 12. (A) Map of igneous intrusion distribution in the Haizi coal mine. (B) Relationship between coal seam gas pressure and burial depth of the No. 10 coal seam in the II101 and II102 mining areas. (C) Relationship between coal seam gas content and burial depth of the No. 10 coal seam in the II101 and II102 mining areas. (D) Amount of absolute gas emission of different working faces in the II101 and II102 mining areas.

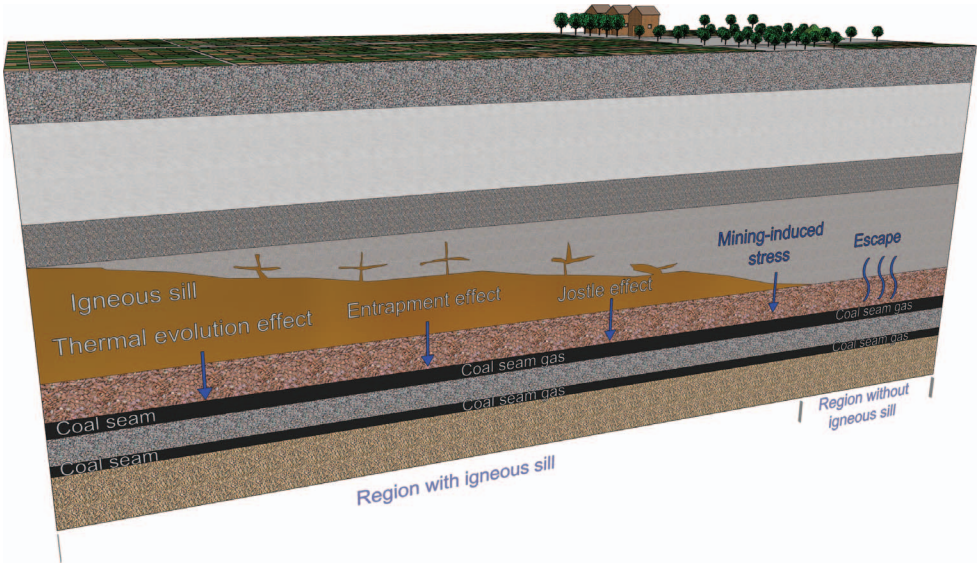

Figure 13. Sketched map of the effects of the extremely thick igneous sill on coal seam gas occurrence and gas hazards in the Haizi coal mine.

released from the working face in the II102 mining area than is released in the II101 mining area during actual mining. Hence, the comparison between these parameters for the II101 and II102 mining areas shows that the No. 10 coal seam in the II102 mining area carries a greater outburst risk. A coal and gas outburst accident occurred on the II1026 working face of the II102 mining area on April 25, 2009. The outburst volumes of coal and gas were 656 t and 13,210 m^3, respectively. No outburst accident occurred in the II101 mining area.

The influence of the igneous sill on underlying coal seam gas occurrence can be summarized as follows. First, as a result of the thermal evolution of the igneous sill, the well-developed pores of coal closer to the sill favor the enhancement of adsorption and desorption capacities. The initial released gas possesses a larger expansion energy after the pressure is released, making it prone to cause coal and gas outbursts (Hu and Wen, 2013). Second, owing to the thermal effect of the igneous sill, the affected coal seams are characterized by relatively high metamorphic grade and gas production, such that their gas content and pressure are larger than those coal seams without sill covering. Third, the igneous sill can restrain coal seam gas emissions and thus exert a well trap effect on coal seam gas due to its low permeability and great thickness. Hence, the igneous sill has significant influence on the generation and storage of coal seam gas in the underlying coal seams, thus significantly increasing the risk of gas hazards in the Haizi coal mine.

Additionally, the jostle effect of the intruded igneous rock on the underlying coal seams leads to the development of occasional tectonically deformed coal layers (Zhang et al., 2015). Rupture of the overlying thick and hard sill can also result in pronounced mining-induced stress during coal seam extraction, which plays an important role in the occurrence of coal and rock outbursts (Wang et al., 2013). In this case, the combined effects of thermal evolution and entrapment make gas hazards more likely to occur in the underlying coal seams as a consequence of the effects of intrusive jostling and mining-induced stress (Figure 13).

CONCLUSIONS

1) The metamorphic grade and methane adsorption capacity of the coal samples increase closer to the sill. Hence, the thermal effect of the igneous sill significantly promotes metamorphism of the affected coal.
2) Owing to the thermal effect of the sill, the pore volume and specific surface area of the coal samples increase progressively closer to the sill, and the coal samples present different pore shapes and pore size distributions. The hysteresis loops suggest the presence of a considerable number of slit-shaped pores in coal samples HZ1 and HZ2 (No. 7 seam and No. 9 seam), which are closer to the sill, indicating better pore connectivity, whereas many semi-closed pores exist in samples HZ3 and HZ4 (situated farther away from the sill) and in sample HZ5 (absent sill covering) of the No. 10 seam, indicating poor connectivity. In addition, the PSDs show that samples HZ1 and HZ2 exhibit a prominent enhancement of the volume of micro-pores and some meso-pores (<5 nm), suggesting significant enhancement of the gas

adsorption and storage capacities of the coal closer to the igneous sill.

3) Under the experimental conditions, effective diffusivity increases closer to the sill and is highly correlated with pore volumes in the size range of 1.1 to 100 nm. In addition, the values of the methane desorption indexes also tend to increase in the coals approaching the sill. The thermal effect of the sill promotes the development of pores in the affected coal, thereby leading to better pore connectivity, enhanced gas adsorption capacity, greater quantities of desorbed gas, and much higher gas desorption and diffusion rates. Consequently, the thermal influence of the igneous sill changes the characteristics of coal seam gas occurrence as a result of the entrapment effect of the extremely thick sill, making gas hazards a recurring problem in the affected coal seams.

ACKNOWLEDGMENTS

This work was supported by the Fundamental Research Funds for the Central Universities (No. 2015XKMS008), the National Science Foundation of China (No. 51574229), Jiangsu Overseas Research & Training Program for University Prominent Young & Middle-Aged Teachers and Presidents, and A Project Funded by the Priority Academic Program Development of Jiangsu Higher Education Institutions (PAPD). We appreciate the helpful comments from the editors and the reviewers.

REFERENCES

Airey, E. M., 1968, Gas emission from broken coal. An experimental and theoretical investigation: *International Journal Rock Mechanics Mining Sciences & Geomechanics Abstracts*, Vol. 5, pp. 475–494.

An, F. H.; Cheng, Y. P.; Wu, D. M.; and Wang, L., 2013, The effect of small micropores on methane adsorption of coals from northern China: *Adsorption*, Vol. 19, pp. 83–90.

Banerjee, B., 1988, Spacing of fissuring network and rate of desorption of methane from coals: *Fuel*, Vol. 67, pp. 1584–1586.

Cai, Y. D.; Liu, D. M.; Pan, Z. J.; Yao, Y. B.; Li, J. Q.; and Qiu, Y. K., 2013, Pore structure and its impact on CH_4 adsorption capacity and flow capability of bituminous and subbituminous coals from northeast China: *Fuel*, Vol. 103, pp. 258–268.

Chen, H. D.; Jiang, J. Y.; Chen, X. J.; and Xu, C., 2014, Differences in coal bed methane occurrence for different regions of igneous erosion in the Haizi coal mine, Huaibei coalfield, China: *Journal Natural Gas Science Engineering*, Vol. 21, pp. 732–737.

Chen, J.; Liu, G. J.; Li, H.; and Wu, B., 2014, Mineralogical and geochemical responses of coal to igneous intrusion in the Pansan coal mine of the Huainan coalfield, Anhui, China: *International Journal Coal Geology*, Vol. 124, pp. 11–35.

Chen, X. J. and Cheng, Y. P., 2015, Influence of the injected water on gas outburst disasters in coal mine: *Natural Hazards*, Vol. 76, pp. 1093–1109.

Cheng, L. B.; Wang, L.; Cheng, Y. P.; Jin, K.; Zhao, W.; and Sun, L. S., 2016, Gas desorption index of drill cuttings affected by magmatic sills for predicting outbursts in coal seams: *Arabian Journal Geosciences*, Vol. 9, pp. 1–15.

Cheng, Y. P.; Wang, H. F.; Wang, L.; Zhou, H. X.; Liu, H. B.; Wu, D. M.; and Li, W., 2010, *Theories and Engineering Applications on Coal Mine Gas Control*: China University of Mining and Technology Press, Xuzhou City, China, 840 p.

Cooper, J. R.; Crelling, J. C.; Rimmer, S. M.; and Whittington, A. G., 2007, Coal metamorphism by igneous intrusion in the Raton Basin, CO and NM: Implications for generation of volatiles: *International Journal Coal Geology*, Vol. 71, pp. 15–27.

Crank, J., 1979, *The Mathematics of Diffusion*: Oxford University Press, London, U.K. 414 p.

Dai, S. F. and Ren, D. Y., 2007, Effects of magmatic intrusion on mineralogy and geochemistry of coals from the Fengfeng-Handan coalfield, Hebei, China: *Energy & Fuels*, Vol. 21, pp. 1663–1673.

Diamond, W. P. and Schatzel, S. J., 1998, Measuring the gas content of coal: A review: *International Journal Coal Geology*, Vol. 35, pp. 311–331.

Du, B., 1985, The initial gas desorption rate as an index of burst of coal and gas: About the parameter of K_t (Chinese translation): *Safety Coal Mines*, Vol. 5, pp. 56–63.

Finkelman, R. B.; Bostick, N. H.; Dulong, F. T.; Senftle, F. E.; and Thorpe, A. N., 1998, Influence of an igneous intrusion on the inorganic geochemistry of a bituminous coal from Pitkin County, Colorado: *International Journal Coal Geology*, Vol. 36, pp. 223–241.

Golab, A. N. and Carr, P. F., 2004, Changes in geochemistry and mineralogy of thermally altered coal, Upper Hunter Valley, Australia: *International Journal Coal Geology*, Vol. 57, pp. 197–210.

Groen, J. C.; Peffer, L. A.; and Pérez-Ramírez, J., 2003, Pore size determination in modified micro- and mesoporous materials. Pitfalls and limitations in gas adsorption data analysis: *Microporous Mesoporous Materials*, Vol. 60, pp. 1–17.

Guo, J. Q.; Kang, T. H.; Kang, J. T.; Zhao, G. F.; and Huang, Z. M., 2014, Effect of the lump size on methane desorption from anthracite: *Journal Natural Gas Science Engineering*, Vol. 20, pp. 337–346.

Han, S. F., 1990, *Geological Condition and Prediction of Coal Accumulation in Huainan and Huaibei Coalfields*: Geological Publishing House, Beijing, 234 p.

Hodot, B., 1966, *Coal and Gas Outbursts (Chinese translation)*: China Coal Industry Press, Beijing, 317 p.

Hu, Q.T. and Wen, G.C., 2013, *Mechanical Mechanism of Coal and Gas Outburst*: Science Press, Beijing, 473 p.

Jian, K.; Lei, D. J.; Fu, X. H.; Zhang, Y. G.; and Li, H. L., 2015, Effect of an electrostatic field on gas adsorption and diffusion in tectonic coal: *International Journal Mining Science and Technology*, Vol. 25, pp. 607–613.

Jiang, J. Y.; Cheng, Y. P.; Wang, L.; Li, W.; and Wang, L., 2011, Petrographic and geochemical effects of sill intrusions on coal and their implications for gas outbursts in the Wolonghu mine, Huaibei coalfield, China: *International Journal Coal Geology*, Vol. 88, pp. 55–66.

Jiang, W. P.; Cui, Y. J.; Zhang, Q.; and Li, Y. H., 2006, The quantum chemical study on the coal surface interacting with CH_4 and CO_2: *Journal China Coal Society*, Vol. 31, pp. 237–240.

Jiang, W. P.; Song, X. Z.; and Zhong, L. W., 2011, Research on the pore properties of different coal body structure coals

and the effects on gas outburst based on the low-temperature nitrogen adsorption method: *Journal China Coal Society*, Vol. 36, pp. 609–614.

Kondo, S.; Ishikawa, T.; and Abe, I., 2005, *Adsorption Science (Chinese translation)*: Chemical Industry, Beijing, 273 p.

Li, X. C.; Nie, B. S.; Zhang, R. M.; and Chi, L. L., 2012, Experiment of gas diffusion and its diffusion mechanism in coal: *International Journal Mining Science Technology*, Vol. 22, pp. 885–889.

Liu, H. H.; Mou, J. H.; and Cheng, Y. P., 2015, Impact of pore structure on gas adsorption and diffusion dynamics for long-flame coal: *Journal Natural Gas Science Engineering*, Vol. 22, pp. 203–213.

Lowell, S.; Shields, J. E.; Thomas, M. A.; and Thommes, M., 2012, *Characterization of Porous Solids and Powders: Surface Area, Pore Size and Density*: Springer Science & Business Media, New York, 339 p.

Lu, S. Q.; Cheng, Y. P.; Qin, L. M.; Li, W.; Zhou, H. X.; and Guo, H. J., 2015, Gas desorption characteristics of the high-rank intact coal and fractured coal: *International Journal Mining Science Technology*, Vol. 25, pp. 819–825.

Marecka, A. and Mianowski, A., 1998, Kinetics of CO_2 and CH_4 sorption on high rank coal at ambient temperatures: *Fuel*, Vol. 77, pp. 1691–1696.

Mastalerz, M.; Drobniak, A.; and Schimmelmann, A., 2009, Changes in optical properties, chemistry, and micropore and mesopore characteristics of bituminous coal at the contact with dikes in the Illinois Basin: *International Journal Coal Geology*, Vol. 77, pp. 310–319.

Mastalerz, M.; He, L.; Melnichenko, Y. B.; and Rupp, J. A., 2012, Porosity of coal and shale: Insights from gas adsorption and SANS/USANS techniques: *Energy & Fuels*, Vol. 26, pp. 5109–5120.

Nie, B. S.; He, X. Q.; and Wang, E. Y., 2000, Diffusion mode of methane gas in coal pores: *Mining Safety & Environment Protection*, Vol. 27, pp. 14–16.

Nie, B. S.; Liu, X. F.; Yang, L. L.; Meng, J. Q.; and Li, X. C., 2015, Pore structure characterization of different rank coals using gas adsorption and scanning electron microscopy: *Fuel*, Vol. 158, pp. 908–917.

Okolo, G. N.; Everson, R. C.; Neomagus, H. W.; Roberts, M. J.; and Sakurovs, R., 2015, Comparing the porosity and surface areas of coal as measured by gas adsorption, mercury intrusion and SAXS techniques: *Fuel*, Vol. 141, pp. 293–304.

Qu, Z. H.; Jiang, B.; Wang J. L.; and Li, M., 2008, Characteristics of tectonic evolution and its controlling effects on coal and gas in Huaibei area: *Coal Geology China*, Vol. 20, pp. 34–37.

Rahman, M. W. and Rimmer, S. M., 2014, Effects of rapid thermal alteration on coal: Geochemical and petrographic signatures in the Springfield (No. 5) coal, Illinois Basin: *International Journal Coal Geology*, Vol. 131, pp. 214–226.

Rimmer, S. M.; Yoksoulian, L. E.; and Hower, J. C., 2009, Anatomy of an intruded coal, I: Effect of contact metamorphism on whole-coal geochemistry, Springfield (No. 5) (Pennsylvanian) coal, Illinois Basin: *International Journal Coal Geology*, Vol. 79, pp. 74–82.

Sachsenhofer, R. F.; Privalov, V. A.; and Panova, E. A., 2012, Basin evolution and coal geology of the Donets Basin (Ukraine, Russia): An overview: *International Journal Coal Geology*, Vol. 89, pp. 26–40.

Saghafi, A.; Pinetown, K. L.; Grobler, P. G.; and Van Heerden, J. H. P., 2008, CO_2 storage potential of South African coals and gas entrapment enhancement due to igneous intrusions: *International Journal Coal Geology*, Vol. 73, pp. 74–87.

Sarana, S. and Kar, R., 2011, Effect of igneous intrusive on coal microconstituents: Study from an Indian Gondwana coalfield: *International Journal Coal Geology*, Vol. 85, pp. 161–167.

Shepherd, J.; Rixon, L. K.; and Griffiths, L., 1981, Outbursts and geological structures in coal mines: A review: *International Journal Rock Mechanics Mining Sciences & Geomechanics Abstracts*, Vol. 18, pp. 267–283.

Skoczylas, N.; Dutka, B.; and Sobczyk, J., 2014, Mechanical and gaseous properties of coal briquettes in terms of outburst risk: *Fuel*, Vol. 134, pp. 45–52.

Stewart, A.; Massey, M.; Padgett, P.; Rimmer, S.; and Hower, J., 2005, Influence of a basic intrusion on the vitrinite reflectance and chemistry of the Springfield (No. 5) coal, Harrisburg, Illinois: *International Journal Coal Geology*, Vol. 63, pp. 58–67.

Thommes, M.; Kaneko, K.; Neimark, A. V.; Olivier, J. P.; Rodriguez-Reinoso, F.; Rouquerol, J.; and Sing, K. S., 2015, Physisorption of gases, with special reference to the evaluation of surface area and pore size distribution (IUPAC Technical Report): *Pure and Applied Chemistry*, Vol. 87, pp. 1051–1069.

Wang, L.; Cheng, L. B.; Cheng, Y. P.; Xu, C.; and Wang, W., 2014a, Influence of thermal events of magma intrusion on coal seams metamorphic grade and adsorption and desorption characteristics: *Journal China Coal Society*, Vol. 39, pp. 1275–1282.

Wang, L.; Cheng, L. B.; Cheng, Y. P.; Yin, G. Z.; Cai, C. C.; Xu, C.; and Jin, K., 2014b, Thermal effects of magmatic sills on coal seam metamorphism and gas occurrence: *Bulletin Volcanology*, Vol. 76, pp. 1–16.

Wang, L.; Cheng, L. B.; Cheng, Y. P.; Yin, G. Z.; Xu, C.; Jin, K.; and Yang, Q. L., 2014c, Characteristics and evolutions of gas dynamic disaster under igneous intrusions and its control technologies: *Journal Natural Gas Science Engineering*, Vol. 18, pp. 164–174.

Wang, L.; Cheng, Y. P.; An, F. H.; Zhou, H. X.; Kong, S. L.; and Wang, W., 2014d, Characteristics of gas disaster in the Huaibei coalfield and its control and development technologies: *Natural Hazards*, Vol. 71, pp. 85–107.

Wang, L.; Cheng, Y. P.; Xu, C.; An, F. H.; Jin, K.; and Zhang, X. L., 2013, The controlling effect of thick-hard igneous rock on pressure relief gas drainage and dynamic disasters in outburst coal seams: *Natural Hazards*, Vol. 66, pp. 1221–1241.

Winter, K. and Janas, H., 1975, Gas emission characteristics of coal and methods of determining the desorbable gas content by means of desorbometers.*: In 16th International Conference on Coal Mine Safety Research, Sept*. 22–26: Washington, D.C.

Wu, D.; Liu, G. J.; Sun, R. Y.; and Chen, S. C., 2014, Influences of magmatic intrusion on the macromolecular and pore structures of coal: Evidences from Raman spectroscopy and atomic force microscopy: *Fuel*, Vol. 119, pp. 191–201.

Xu, C.; Cheng, Y. P.; Ren, T.; Wang, L.; Kong, S. L.; and Lu, S. Q., 2014, Gas ejection accident analysis in bed splitting under igneous sills and the associated control technologies: A case study in the Yangliu mine, Huaibei coalfield, China: *Natural Hazards*, Vol. 71, pp. 109–134.

Xu, H.; Tang, D. Z.; Zhao, J. L.; Li, S.; and Tao, S., 2015, A new laboratory method for accurate measurement of the methane diffusion coefficient and its influencing factors in the coal matrix: *Fuel*, Vol. 158, pp. 239–247.

Yang, F.; Ning, Z. F.; and Liu, H. Q., 2014, Fractal characteristics of shales from a shale gas reservoir in the Sichuan Basin, China: *Fuel*, Vol. 115, pp. 378–384.

Yang, M.; Liu, G. J.; Sun, R. Y.; Chou, C. L.; and Zheng, L. G., 2012, Characterization of intrusive rocks and REE geochemistry of coals from the Zhuji coal mine, Huainan coalfield, Anhui, China: *International Journal Coal Geology*, Vol. 94, pp. 283–295.

Yang, Q.; Wu, C. L.; and Tang, D. Z., 1996, *Coal Metamorphism in China*: China Coal Industry Publishing House, Beijing, 212 p.

Yao, Y. B. and Liu, D. M., 2012, Effects of igneous intrusions on coal petrology, pore-fracture and coalbed methane characteristics in Hongyang, Handan and Huaibei coalfields, North China: *International Journal Coal Geology*, Vol. 96, pp. 72–81.

Yao, Y. B.; Liu, D. M.; and Huang, W. H., 2011, Influences of igneous intrusions on coal rank, coal quality and adsorption capacity in Hongyang, Handan and Huaibei coalfields, North China: *International Journal Coal Geology*, Vol. 88, pp. 135–146.

Zhang, D. F.; Gu, L. L.; Li, S. G.; Lian, P. C.; and Tao, J., 2013, Interactions of supercritical CO_2 with coal: *Energy & Fuels*, Vol. 27, pp. 387–393.

Zhang, X. L.; Cheng, Y. P.; Wang, L.; and Zhao, W., 2015, Research on the controlling effects of a layered sill with different thicknesses on the underlying coal seam gas occurrence: *Journal Natural Gas Science Engineering*, Vol. 22, pp. 406–414.

Zhang, Y. X., 2008, *Geochemical Kinetics*: Princeton University Press, Princeton, NJ, 631 p.